On the derivation of a spatially distributed aerosol climatology for its incorporation in a radiometric Landsat pre-processing framework

D. Frantz[*1], A. Röder[1], M. Stellmes[1] and J. Hill[1]

[1] *Environmental Remote Sensing and Geoinformatics, Trier University, Trier, Germany*

* corresponding author: David Frantz, e-Mail: frantz@uni-trier.de

The Version of Record of this manuscript has been published and is available in Remote Sensing Letters, published online on 20 July, 2015, http://www.tandfonline.com/doi/abs/10.1080/2150704X.2015.1070314

Reference:
D. Frantz; A. Röder; M. Stellmes; J. Hill (2015), "On the derivation of a spatially distributed aerosol climatology for its incorporation in a radiometric Landsat pre-processing framework," in *Remote Sensing Letters*, vol. 6, iss. 8, pp. 647-656.

DOI: 10.1080/2150704X.2015.1070314
Online available at:
http://www.tandfonline.com/doi/abs/10.1080/2150704X.2015.1070314

This work was funded within the Southern African Science Service Centre for Climate Change and Adaptive Land Management project by the Federal Ministry of Education and Research.

On the derivation of a spatially distributed aerosol climatology for its incorporation in a radiometric Landsat pre-processing framework

We developed a spatio-temporal path reflectance climatology for use in atmospheric corrections for a Landsat pre-processing framework. The climatology is intended as a fallback strategy for aerosol estimation in bright Southern African savannah ecosystems where the rarity of dark objects decreases the applicability of common image-based aerosol estimation strategies and the widespread burning prohibits the use of a fixed aerosol loading. We predicted the climatological path reflectance surface by applying a multivariate regression model to all available path reflectance retrievals on basis of the geolocation and the days of the year on which the data were acquired. The resulting predictions are able to successfully model major spatio-temporal gradients of the path reflectance distribution. The prediction error (weighted RMSE at 0.483 µm) was less than 1% reflectance while the prediction itself varied by 4.6% reflectance. Thus, using the modelled climatology for atmospheric correction is favourable compared to a fixed aerosol content.

Keywords: aerosol; Landsat; large area; multitemporal; Southern Africa

1. Introduction

Recent advances in open data policies (Woodcock et al. 2008) have drastically changed the use of Landsat data and encouraged the development of mass-processing frameworks (Wulder et al. 2012). Concurrently, the use of an increasing amount of Landsat images also raised the demands on the radiometric processing quality and on the derivation of ready-to-use standard products (Hansen and Loveland 2012). Currently, radiative transfer modelling (e.g. Tanré et al. 1979) is agreed to be the quasi-standard in radiometric corrections and as such the estimation of aerosol optical depth (AOD) becomes a key parameter due to its profound impact on biophysical parameters (Gillingham, Flood, and Gill 2012). State-of-the-art large area generation systems like the widely used LEDAPS approach (Landsat Ecosystem Disturbance Adaptive Processing System, Masek et al. 2006) estimate the AOD directly from the imagery. It is assumed that a few virtually zero reflectance pixels exist in every image (Hill and Sturm 1991) and the aerosol loading is commonly derived by applying the dark, dense vegetation method (DDV, e.g. Kaufman and Sendra 1988) or the dark object subtraction approach (DOS, e.g. Moran et al. 1992, Chavez 1996). Whilst these are generally accepted approaches, the estimation of AOD with dark object methods is not usable if there are no suitable targets. Kaufman and Sendra (1988) already identified regions where the large-scale absence of dark vegetation restricts the operational usage of the DDV approach, which applies for some larger parts of our study area in the bright Southern African savannahs. Gillingham et al. (2011) already documented the inability to operationally apply the DDV under the similar Australian conditions which led to the decision of simply fixing the AOD to a reasonable value in the Eastern Australian Landsat pre-processing scheme (Flood et al. 2013). Nevertheless, it is more desirable to correct each image with a more appropriate atmospheric parameter set, which is especially mandatory if the assumption of a stable AOD is violated. Southern African savannahs are amongst the most fire-prone and most frequently burnt ecosystems in the world (Bond and Keeley 2005) and as such substantial seasonal and spatial variations in aerosol loadings are prevalent (Eck et al. 2001).

We report on the derivation of a spatially explicit path reflectance climatology for its intended use in an operational pre-processing framework as a substitute for

occasionally erroneous image-based path reflectance and AOD estimations in the case that meaningful dark objects cannot be identified in a given image. This climatology generates a smooth surface from the surrounding reliable retrieved path reflectance values, thus bridging the gaps where the image-based aerosol characterization failed. The corrected Landsat data are intended to be used in a pixel-based compositing application in the context of wall-to-wall deforestation and forest degradation assessments, as well as being intended for time series applications in general.

2. Methods

2.1 Background

We implemented an operational large-area pre-processing framework for the generation of multi-sensor surface reflectance Landsat datasets (Frantz et al., in submission). The approach includes methods for the automatic detection of clouds and cloud shadows (Zhu and Woodcock 2012, Zhu, Wang, and Woodcock 2015), functions for reprojecting the data to a shared coordinate system and the partitioning of the data to gridded data structure. The radiometric correction includes a C-correction for terrain normalization (Kobayashi and Sanga-Ngoie 2008, Teillet, Guindon, and Goodenough 1982). The atmospheric correction module is based on Tanré's formulation of the radiative transfer (Tanré et al. 1979) and includes adjacency effect correction, the correction of water vapour absorption by a MODIS-derived (Moderate Resolution Imaging Spectroradiometer) water vapour database and a joint database- and image-based estimation of AOD over dark objects. The employed dark object database holds information on the temporal persistence of dark objects and was generated by an exhaustive analysis of all available uncorrected Landsat images. The darkest pixels were identified in each image and the dark object persistency (DOP = [0 … 100], i.e. the percentage of the time a pixel is dark) is derived for each pixel in the study area. The most permanent objects are then favoured in the actual radiometric processing for the path reflectance estimation. The usage of the DOP substantially increases the quality of retrieved values over the dark objects because transient dark features like temporal flooding or burnt areas are successfully rejected while perennial water bodies or topographic shadows are favoured. A visualization of the DOP for two sample areas is appended as electronic material in the "figshare" section. We processed all available 57,371 Level 1T Landsat images for Angola, Zambia, Zimbabwe, Botswana and Namibia and recorded the estimated path reflectance ρ_p, on which our prediction model is based. The path reflectance is closely related to AOD (Hill and Sturm 1991), which can be inferred with a scattering model (e.g. the multiple scattering approximation, Sobolev 1975) as demonstrated in (Frantz et al., in submission).

2.2 Observations

We successfully characterized the scattering effects for the majority of the Landsat images with this approach. Nevertheless, we encountered serious problems in deriving AOD for a substantial number of Landsat images (~43% of all images), which especially was a problem in southern Namibia and Botswana where the dry season surface is bright and dark objects are rare or not apparent at all. Therefore, we closely investigated the seasonal and spatial patterns of the 57% successful ρ_p estimates. Figure 1 depicts ρ_p for an illustrative Landsat frame at the Namibian/Angolan border that includes the perennial Cubango and Cuito rivers. The retrieved ρ_p values in this frame were of high quality and

all depicted points were estimated from permanent dark objects, i.e. objects that are the darkest pixels in the given scene over time. There is a clear seasonal pattern, which is especially pronounced in the visible bands, where the effect of aerosols is most prominent. The depicted region follows the typical southern African climate with two main seasons, i.e. a wet and a dry season. The dry season begins in May and lasts until September, though the hottest temperatures are not reached until October, when the rainfall sums are also still relatively low (Weber 2013). Path reflectance values are small during the wet season and begin to increase with the onset of the dry season. The increase continues until the approximate end of the dry season in September/October after which the values quickly drop back to the wet season base value.

Please place Figure 1 approximately here.

In addition to the temporal pattern, we also identified spatial dependencies. Figure 2 displays mean ρ_p values for the blue wavelength band for the dry season acquisition months. The aerosol accumulation apparently starts earlier in North-western Angola and progresses towards Botswana in the South-Eastern part of the region. The aerosol depletion also starts earlier in North-Western Angola while the highest loadings are found in the centre of the study area in the late dry season. Overall, the amplitude of the aerosol accumulation is lowest in the South. Figure 2 also indicates the Landsat frames where the identification of dark objects failed, which are especially the southern dry savannah ecotypes, whereas reliable estimates were retrieved in the darker regions, e.g. the Okavango catchment area. In addition, some frames in northern Angola are also suspect of missing data, though this is due to a substantial decrease in data availability because of persistent cloud overcast in the tropics.

Please place Figure 2 approximately here.

2.3 Modelling

As a consequence of the observed temporal and spatial patterns, we aimed at generating a spatially distributed ρ_p climatology, modelled from the available data. This climatology is intended to be used as fallback strategy in the implemented Landsat pre-processing framework when actual AOD cannot be retrieved from dark targets.

A multivariate regression model described by the geolocation – coordinates (X,Y) - and the acquisition day-of-year (DOY) of the 57% successful ρ_p estimates was employed for every Landsat band b:

$$\begin{aligned}\rho_{p,b} = {} & c_0 + c_1X + c_2Y + c_3XY + c_4X^2 + c_5Y^2 + c_6(\mathrm{DOY}) + c_7(\mathrm{DOY})^2 + \\ & c_8X\sin(2\pi(\mathrm{DOY})/365) + c_9X\cos(2\pi(\mathrm{DOY})/365) + \\ & c_{10}Y\sin(2\pi(\mathrm{DOY})/365) + c_{11}Y\cos(2\pi(\mathrm{DOY})/365) + \\ & c_{12}X\sin(4\pi(\mathrm{DOY})/365) + c_{13}X\cos(4\pi(\mathrm{DOY})/365) + \\ & c_{14}Y\sin(4\pi(\mathrm{DOY})/365) + c_{15}Y\cos(4\pi(\mathrm{DOY})/365) + \\ & c_{16}X\sin(6\pi(\mathrm{DOY})/365) + c_{17}X\cos(6\pi(\mathrm{DOY})/365) + \\ & c_{18}Y\sin(6\pi(\mathrm{DOY})/365) + c_{19}Y\cos(6\pi(\mathrm{DOY})/365).\end{aligned} \quad (1)$$

The DOP (in %, see also Figure 3) was used to weight the observations during the estimation of the regression coefficients $c_{0\text{-}19}$ by the means of weighted least squares fitting. We assumed that temporally persistent dark objects are more reliable for characterizing atmospheric scattering effects due to their inherent pseudo-invariant

reflectance, which is often exploited for improving atmospheric correction methods (Themistocleous et al. 2013). The coefficient c_0 is the path reflectance intercept; the coefficients $c_{1\text{-}5}$ explain purely spatial trends on the path reflectance, whereas the coefficients $c_{6\text{-}7}$ explain the non-interacting temporal trend. The remaining coefficients describe combined spatio-temporal effects by modelling seasonal cycles of varying frequency with geolocation-dependency. As a boundary condition, the prediction is enforced to be cyclic by twofold data repetition yielding three identical annual cycles.

3. Results

Table 1 summarizes ρ_p prediction errors for the employed spatio-temporal model, i.e. the Mean Error (ME) as a measure for the prediction bias, the Mean Absolute Error (MAE*)*, the Root Mean Squared Error (RMSE*)* and its weighted counterpart (WRMSE*)*.

The ME indicate that the residuals e_i are close to zero and have a small bias. The bias is largest in the blue wavelength band. The MAE, RMSE and WRMSE all report similar errors and the errors for the first four wavelengths are very similar and in the order of 1% reflectance. The MAE values are smallest and RMSE values are the greatest due to the stronger contribution of outliers. The WRMSE might be the most appropriate measure for quantifying the goodness of the fit since we also employed a weighted prediction.

Please place Table 1 approximately here.

Figure 3 depicts the blue wavelength ρ_p retrievals (points) for one path of Landsat data (one orbit in approximate North-South direction), as well as the resulting prediction (line). The prediction successfully modelled the main seasonal and latitudinal variations in ρ_p. It is also apparent that there are fluctuations and outliers around the modelled fit, which surely affect the prediction errors shown in Table 1. Figure 4 summarizes the latitude dependency of several key parameters of the data show in Figure 3. Figure 4 (*a*) corroborates the previous finding that the aerosol peaking is delayed in the south. The maximum values (Figure 4 *b*) are found at medium latitudes, though this might be different in other orbital slices in the study area. Concurrently, the minimum predictions (Figure 4 *c*) increase southwards, indicating a higher base level of aerosol loading.

Please place Figure 3 approximately here.

Please place Figure 4 approximately here.

We inferred the aerosol optical depth at 483 µm from the modelled ρ_p climatology by using the multiple scattering approximation (Frantz et al., in submission). Figure 5 illustrates the spatial AOD surfaces for selected dates in the dry season. The prediction resulted in a smooth and seamless AOD surface for the entire study area and corroborates the earlier findings, i.e. (1) an earlier onset in aerosol accumulation in the North, (2) stronger aerosol loadings in the north, (3) earlier aerosol depletion in the north and (4) highest aerosol loadings in the centre of the study area towards the end of the dry season. The complete and animated daily time series of AOD surfaces is appended as electronic material in the “figshare” section of this article.

Please place Figure 5 approximately here.

In order to quantitatively evaluate the goodness of the retrieved ρ_p and AOD values, we compared our results with data from the Aerosol Robotic Network (AERONET). The site at Mongu, Zambia (15.254°S, 23.151°E) is the only station with multiple years of data within our study area. We computed the average seasonal AOD cycle at 0.483 µm and used the corresponding Landsat frame (175/071) for the comparison, see Figure 6. The ME between the AERONET climatology (points) and the inferred AOD climatology (dashed line) is 0.137 which indicates that the path reflectance estimations are systematically too low. We tried to quantitatively assess the underestimation in ρ_p by inverting the multiple scattering computations such that the RMSE between the AERONET and the predicted AOD is minimized: ρ_p is then underestimated by 0.0074 reflectance (dotted line in Figure 6). The AERONET climatology and the offset AOD are very similar.

Please place Figure 6 approximately here.

4. Discussion

Our prediction model generates seamless and smooth ρ_p and AOD surfaces for the entire study area and for each DOY. We intended to model the large-scale spatial path reflectance climatology and aimed to reproduce the major aerosol gradients in the study area. The presented model statistics indicated that the prediction model generally adapts to the input data, but there are also deviations from the underlying data. The weighted RMSE indicated that the prediction error is in the order of 0.01 reflectance for the short wavelength bands. The blue-band ρ_p prediction range (i.e. predicted maximum – minimum) is 0.046 and the input ρ_p range is even higher: 0.07 (99% of the data). Therefore, the prediction error is 4.6 (7) times smaller than the predicted (observed) data range and thus, we conclude that using such a climatology is preferable over using a constant aerosol loading in the radiometric correction. This observation is also supported by the findings of Gillingham, Flood and Gill (2012), who found that a fixed AOD (at 0.5 µm) of 0.05 only ensures reliable results if the actual AOD is less than 0.1. The annual AOD variability is significantly higher in our study area (compare with Figure 5) but a quantitative assessment about the effect on generated products when using a constant vs a climatological aerosol characterization would be useful for future work. Nevertheless, these findings should be verified for other study areas where burning might be less influential. In areas where the AOD is rather stable throughout the year, fixing AOD might be the more practical approach.

In general, aerosol tends to accumulate during the course of the dry season but the onset, end, minimum and maximum of the accumulation are variable. The northern part of the study area is more affected by aerosol. The southern African burning regimes are a major factor in the spatio-temporal distribution of aerosols (Eck et al. 2001). In southern Africa, the seasonality is very strictly partitioned into a wet and a dry season. In the wet season, the aerosol loading is washed out (Eck et al. 2001). In the dry season, burning is very widespread (Stellmes et al. 2013) and the absence of precipitation allows for the accumulation of biomass burning aerosol particles. The burning season starts and stops earlier in the North (Stellmes et al. 2013) and so does the aerosol accumulation. The aerosol loading is also higher, which could be partially caused by the early burns because the potential accumulation time is prolonged. In addition, northern Angola is characterized by the highest fuel loads due to the latitudinal rainfall gradient, which

results in a larger amount of burned biomass and emitted aerosols per burned area if the burning efficiency is assumed to be constant (Scholes, Kendall, and Justice 1996, Barbosa et al. 1999). Smaller amounts of fuel, as well as the late start of the main fire season (Stellmes et al. 2013) could be responsible for the delayed aerosol accumulation and the decreased aerosol loadings in the South and centre of the area.

The comparison between the inferred AOD and AERONET data revealed that our method systematically underestimates ρ_p and AOD. The ρ_p underestimation was less than 1% reflectance but the effect on AOD was clearly visible. AERONET data availability in our study area is very limited (only one site with sufficient data) and as such, we cannot confirm nor verify that this bias globally applies to our data or if there are regional deviations. The initial estimation of the path reflectance was performed in the employed Landsat pre-processing framework (Frantz et al., in submission) where it was attempted to identify the true reflectance of the dark objects. The iteration step for determining the true reflectance was set to 1% reflectance and thus the underestimation of less than 1% could result from this. Potentially, the increase of the iteration resolution would compensate for the underestimation and will be considered in the next re-processing.

While the approach well represents large scale gradients in the aerosol distribution, the generalized model may not adequately resolve local variations at a spatial extension of approximately two Landsat scenes or less. The observed variations (see e.g. Figure 2) could be caused by distinct local fire regimes, the distribution of urban centres and potentially also locally driven deviations from the climate regime, e.g. the occurrence of orographic rainfalls. In addition, uncertainties in estimating ρ_p over dark objects could also add to the heterogeneity. Nevertheless, we aimed at reproducing the large-scale variations in order to provide a regionally adapted alternative to using a fixed aerosol characterization in a radiometric pre-processing scheme and as such, we conclude that the local deviations are acceptable in the practical implementation.

5. Conclusion

We developed a climatology based alternative strategy for coping with variable aerosol loadings under the environmental constraint of absent dark objects in bright ecoregions. Contrary to fixing the aerosol optical depth to a reasonable value, our approach explicitly models the spatio-temporal aerosol distribution from the available surrounding path reflectance estimations and thus reproduces the major large-scale gradients. The predictions are intended to serve as input to an operational radiometric pre-processing framework for the generation of large area surface reflectance Landsat datasets.

Acknowledgement

Landsat data courtesy of the U.S. Geological Survey. We thank the AERONET PI for its effort in establishing and maintaining the Mongu site. We are grateful to two anonymous reviewers whose comments helped improve the manuscript. The SASSCAL project was funded by the Federal Ministry of Education and Research.

References

Barbosa, P.M., D. Stroppiana, J.-M. Grégoire, and J.M. Cardoso Pereira. 1999. "An assessment of vegetation fire in Africa (1981–1991): Burned areas, burned biomass, and atmospheric emissions." *Global Biogeochemical Cycles* 13 (4):933-950. doi: 10.1029/1999gb900042.

Bond, W.J., and J.E. Keeley. 2005. "Fire as a global 'herbivore': the ecology and evolution of flammable ecosystems." *Trends in Ecology & Evolution* 20 (7):387-394. doi: 10.1016/j.tree.2005.04.025.

Chavez, P.S. 1996. "Image-based atmospheric corrections-revisited and improved." *Photogrammetric Engineering and Remote Sensing* 62 (9):1025-1035.

Eck, T.F., B.N. Holben, D. Ward, O. Dubovik, J. Reid, A. Smirnov, M. Mukelabai, N. Hsu, N. O'Neill, and I. Slutsker. 2001. "Characterization of the optical properties of biomass burning aerosols in Zambia during the 1997 ZIBBEE field campaign." *Journal of Geophysical Research: Atmospheres (1984–2012)* 106 (D4):3425-3448. doi: 10.1029/2000JD900555.

Flood, N., T. Danaher, T.K. Gill, and S.S. Gillingham. 2013. "An Operational Scheme for Deriving Standardised Surface Reflectance from Landsat TM/ETM+ and SPOT HRG Imagery for Eastern Australia." *Remote Sensing* 5 (1):83-109. doi: 10.3390/rs5010083.

Frantz, D., A. Röder, M. Stellmes, and J. Hill. "An operational radiometric Landsat pre-processing framework for large area time series applications." *In submission*.

Gillingham, S.S., N. Flood, and T.K. Gill. 2012. "On determining appropriate aerosol optical depth values for atmospheric correction of satellite imagery for biophysical parameter retrieval: requirements and limitations under Australian conditions." *International Journal of Remote Sensing* 34 (6):2089-2100. doi: 10.1080/01431161.2012.738945.

Gillingham, S.S., N. Flood, T.K. Gill, and R.M. Mitchell. 2011. "Limitations of the dense dark vegetation method for aerosol retrieval under Australian conditions." *Remote Sensing Letters* 3 (1):67-76. doi: 10.1080/01431161.2010.533298.

Hansen, M.C., and T.R. Loveland. 2012. "A review of large area monitoring of land cover change using Landsat data." *Remote Sensing of Environment* 122 (0):66-74. doi: 10.1016/j.rse.2011.08.024.

Hill, J., and B. Sturm. 1991. "Radiometric correction of multitemporal Thematic Mapper data for use in agricultural land-cover classification and vegetation monitoring." *International Journal of Remote Sensing* 12 (7):1471-1491. doi: 10.1080/01431169108955184.

Kaufman, Y.J., and C. Sendra. 1988. "Algorithm for automatic atmospheric corrections to visible and near-IR satellite imagery." *International Journal of Remote Sensing* 9 (8):1357-1381. doi: 10.1080/01431168808954942.

Kobayashi, S., and K. Sanga-Ngoie. 2008. "The integrated radiometric correction of optical remote sensing imageries." *International Journal of Remote Sensing* 29 (20):5957-5985. doi: 10.1080/01431160701881889.

Masek, J.G., E.F. Vermote, N.E. Saleous, R. Wolfe, F.G. Hall, K.F. Huemmrich, G. Feng, J. Kutler, and L. Teng-Kui. 2006. "A Landsat surface reflectance dataset for North America, 1990-2000." *IEEE Geoscience and Remote Sensing Letters* 3 (1):68-72. doi: 10.1109/lgrs.2005.857030.

Moran, M.S., R.D. Jackson, P.N. Slater, and P.M. Teillet. 1992. "Evaluation of simplified procedures for retrieval of land surface reflectance factors from satellite sensor output." *Remote Sensing of Environment* 41 (2–3):169-184. doi: 10.1016/0034-4257(92)90076-V.

Scholes, R., J. Kendall, and C. Justice. 1996. "The quantity of biomass burned in southern Africa." *Journal of Geophysical Research: Atmospheres (1984–2012)* 101 (D19):23667-23676.

Sobolev, V.V. 1975. "Light scattering in planetary atmospheres." *(Translation of Rasseianie sveta v atmosferakh planet, Moscow, Izdatel'stvo Nauka, 1972.)*

Oxford and New York, Pergamon Press (International Series of Monographs in Natural Philosophy. Volume 76), 1975. 263 p. 1.

Stellmes, M., D. Frantz, M. Finckh, and R. Revermann. 2013. "Fire frequency, fire seasonality and fire intensity within the Okavango region derived from MODIS fire products." In *Special Volume: Environmental Assessments in the Okavango Region*, edited by Jens Oldeland, Cynthia Erb, Manfred Finckh and Norbert Jürgens.

Tanré, D., M. Herman, P.Y. Deschamps, and A. de Leffe. 1979. "Atmospheric modeling for space measurements of ground reflectances, including bidirectional properties." *Applied Optics* 18 (21):3587-3594. doi: 10.1364/ao.18.003587.

Teillet, P., B. Guindon, and D. Goodenough. 1982. "On the slope-aspect correction of multispectral scanner data." *Canadian Journal of Remote Sensing* 8 (2):84-106. doi: 10.1080/07038992.1982.10855028.

Themistocleous, K., D.G. Hadjimitsis, A. Retalis, N. Chrysoulakis, and S. Michaelides. 2013. "Precipitation effects on the selection of suitable non-variant targets intended for atmospheric correction of satellite remotely sensed imagery." *Atmospheric Research* 131 (0):73-80. doi: 10.1016/j.atmosres.2012.02.015.

Weber, T. 2013. "Mashare - Climate." In *Special Volume: Environmental Assessments in the Okavango Region*, edited by Jens Oldeland, Cynthia Erb, Manfred Finckh and Norbert Jürgens.

Woodcock, C.E., R. Allen, M. Anderson, A. Belward, R. Bindschadler, W. Cohen, F. Gao, S.N. Goward, D. Helder, and E. Helmer. 2008. "Free access to Landsat imagery." *Science* 320 (5879):1011a. doi: 10.1126/science.320.5879.1011a.

Wulder, M.A., J.G. Masek, W.B. Cohen, T.R. Loveland, and C.E. Woodcock. 2012. "Opening the archive: How free data has enabled the science and monitoring promise of Landsat." *Remote Sensing of Environment* 122 (0):2-10. doi: 10.1016/j.rse.2012.01.010.

Zhu, Z., S. Wang, and C.E. Woodcock. 2015. "Improvement and expansion of the Fmask algorithm: cloud, cloud shadow, and snow detection for Landsats 4–7, 8, and Sentinel 2 images." *Remote Sensing of Environment* 159 (0):269-277. doi: 10.1016/j.rse.2014.12.014.

Zhu, Z., and C.E. Woodcock. 2012. "Object-based cloud and cloud shadow detection in Landsat imagery." *Remote Sensing of Environment* 118 (0):83-94. doi: 10.1016/j.rse.2011.10.028.

Figures and Tables

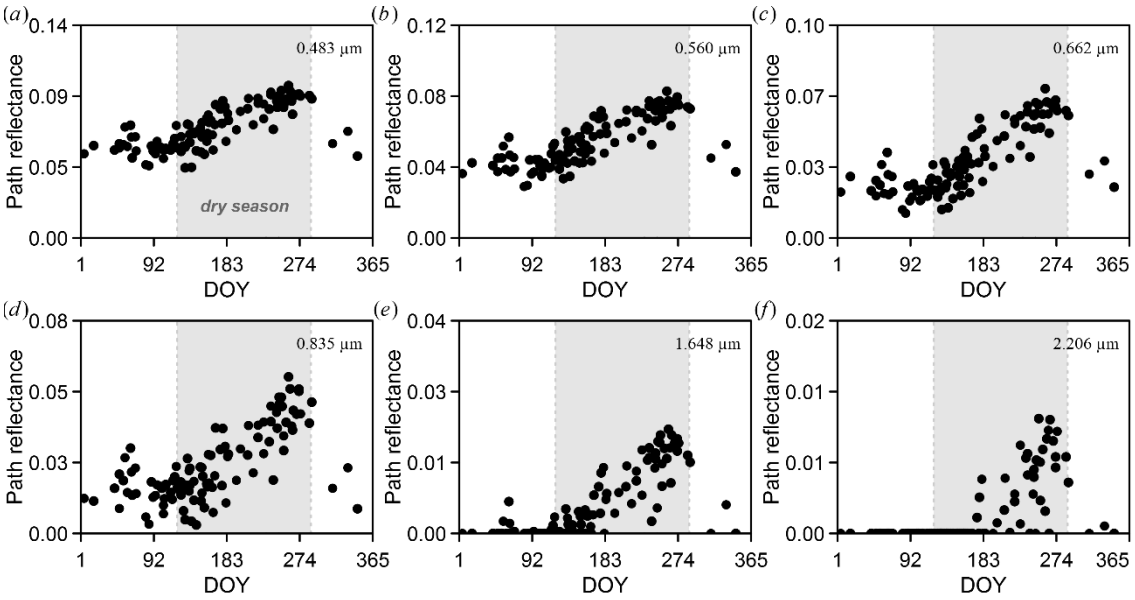

Figure 1. Successful path reflectance retrievals for the six reflective Landsat bands for an illustrative Landsat frame (177/072). The frame is located at the Namibian/Angolan border and includes the perennial Cubango and Cuito rivers. The grey background indicates the dry season.

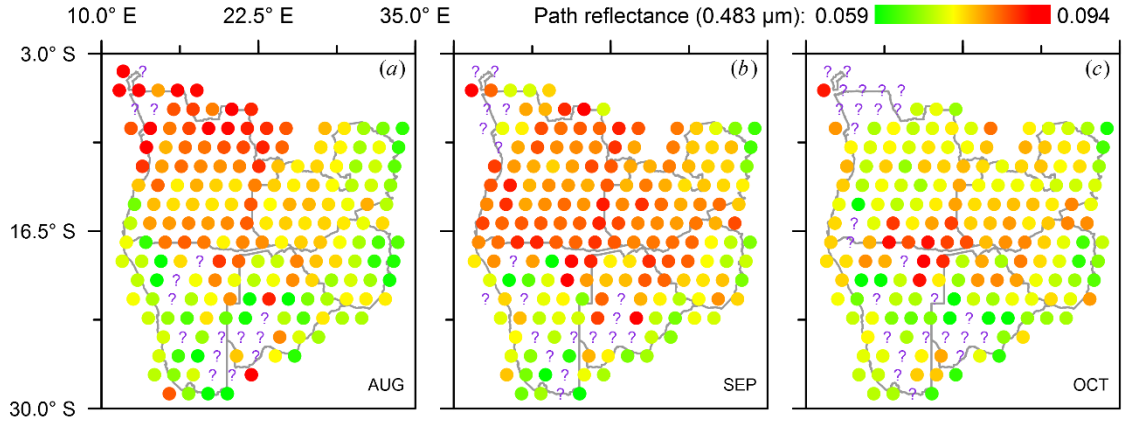

Figure 2. Mean path reflectance retrievals (0.483 µm). Mean values are computed for every Landsat frame for the depicted acquisition months; only the successful retrievals were considered. '?' marks indicate Landsat frames where the dark object identification failed or there were no cloud-free images.

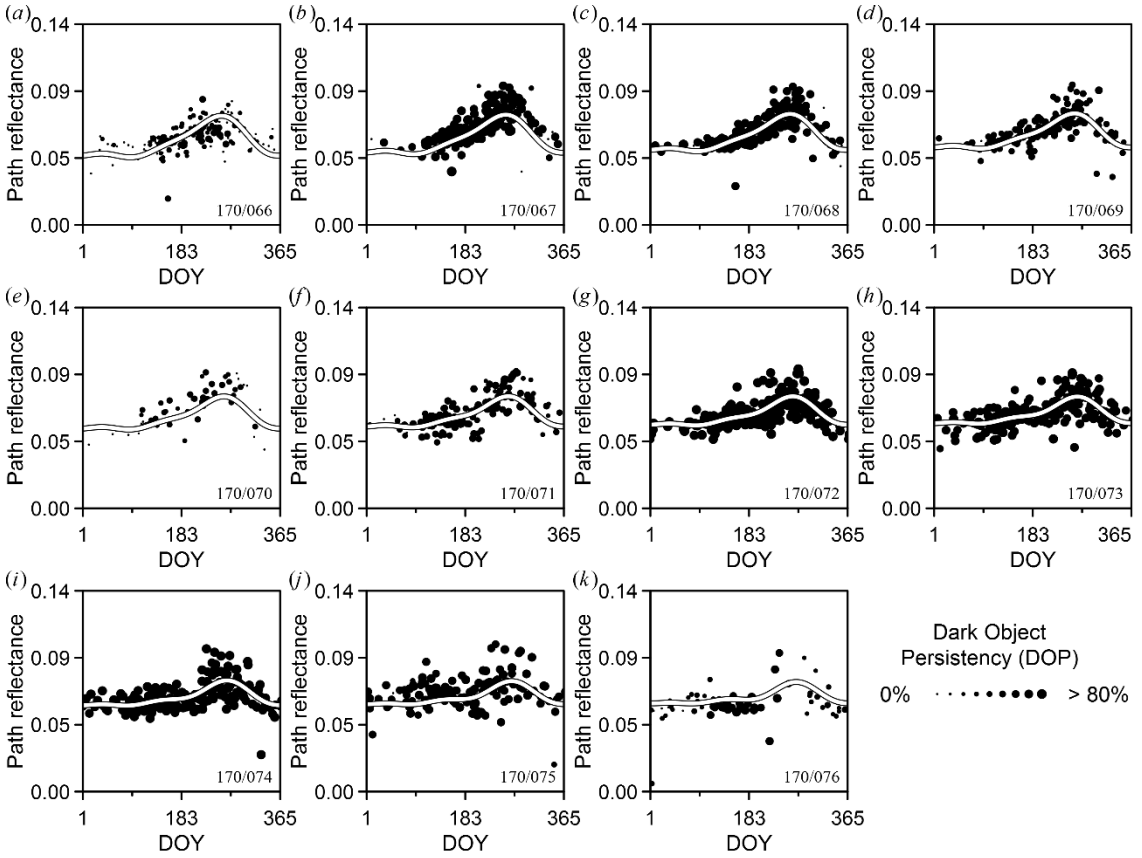

Figure 3. Initial path reflectance retrievals (0.483µm) and prediction (line) for a series of Landsat frames within one orbit (path 170, i.e. in the Eastern part of the study area). The path/row is labelled in the bottom right corner. The persistence of the dark objects (DOP) which were used for estimating the path reflectance is indicated by the variable point size. The persistence was used to weight the observations in the prediction.

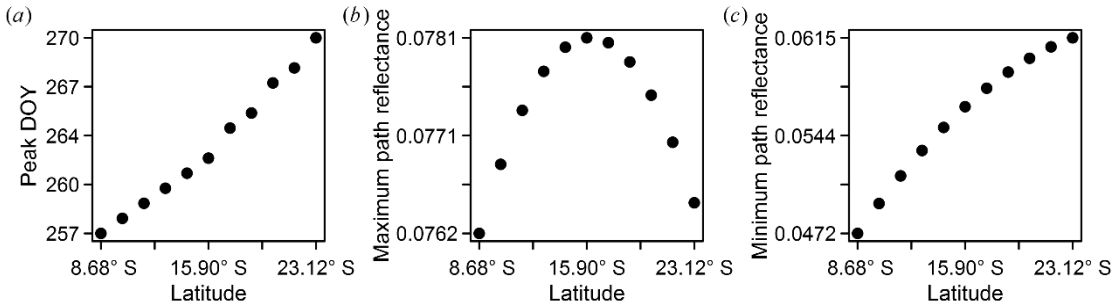

Figure 4. Latitude dependence of (a) the timing of peak aerosol loading, (b) the maximum predicted path reflectance and (c) the minimum predicted path reflectance. The data are inferred from the depicted prediction in Figure 3.

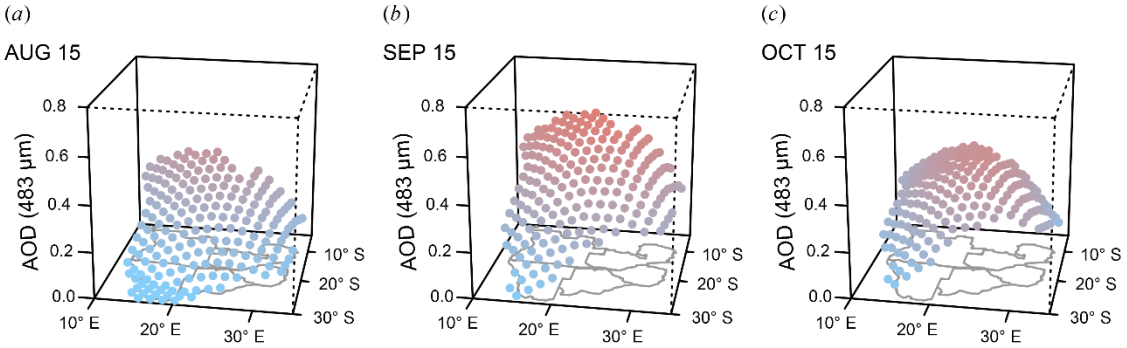

Figure 5. Predicted aerosol optical depth surfaces at 0.483µm for three dates in the dry season; see the online version of this article for the complete and animated time series.

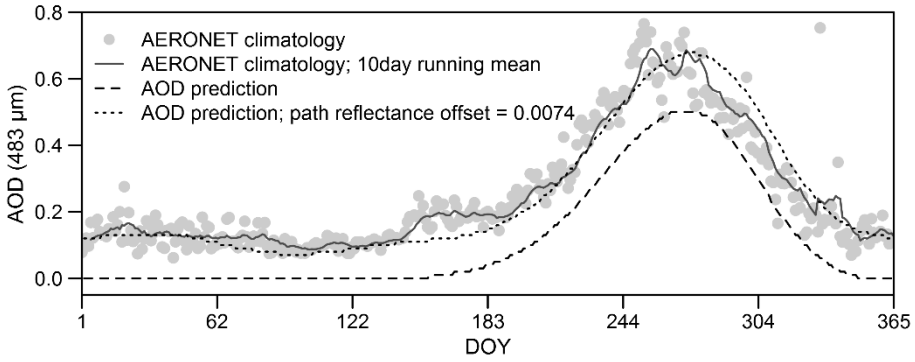

Figure 6. Average annual AOD cycle for the AERONET Mongu site and the corresponding AOD prediction. The path reflectance offset was found by inverting the multiple scattering computation such that the RMSE between the AERONET and the predicted AOD is minimized.

Table 1. Path reflectance prediction errors for every Landsat band: Mean Error (ME), Mean Absolute Error (MAE), Root Mean Squared Error (RMSE) and weighted Root Mean Squared Error (WRMSE). All errors are reported in reflectance units. e_i are the residuals between the model fit and the actual data for every data point i, w_i are the weights used for the prediction.

Wavelength (µm)	Landsat band	ME	MAE	RMSE	WRMSE
		$\sum_{i=1}^{n} e_i/n$	$\sum_{i=1}^{n} \lvert e_i \rvert/n$	$\sqrt{\sum_{i=1}^{n} e_i^2/n}$	$\sqrt{\sum_{i=1}^{n} w_i e_i^2/\sum_{i=}^{n}}$
0.483	Blue	0.00111	0.0080	0.0110	0.0095
0.560	Green	0.00005	0.0080	0.0108	0.0101
0.662	Red	-0.00054	0.0082	0.0109	0.0099
0.835	NIR	-0.00045	0.0080	0.0104	0.0099
1.648	SWIR1	0.00004	0.0020	0.0032	0.0031
2.206	SWIR2	0.00003	0.0006	0.0013	0.0012